

Bismuth Halide Perovskites for CO₂ Photoreduction

Subjects: [Nanoscience & Nanotechnology](#)

Contributor: Edith Luévano-Hipólito , Oscar L. Quintero-Lizárraga , Leticia M. Torres-Martínez

Inspired by natural photosynthesis, the photocatalytic CO₂ reduction reaction (CO₂RR) stands as a viable strategy to produce solar fuels and mitigate the high dependence on highly polluting fossil fuels, as well as to decrease the CO₂ concentration in the atmosphere. The design of efficient photocatalytic materials is crucial to ensure the long-term application of the CO₂RR process. So far, perovskite materials have shown high efficiencies in CO₂RR to generate different solar fuels, specially lead halide perovskites (LHP), which exhibit valuable features for the obtention of high production yields (e.g., narrow band gaps, adequate potentials for CO₂RR, good charge transport properties, etc.). Nonetheless, the presence of lead involves an important environmental impact that cannot be negligible in the design of industrial-scale photocatalytic processes. Hence, the search for efficient Lead-free Halide Perovskites (LFHP) remains a high-priority task in the research of functional materials for CO₂RR, since LFHPs could maintain the properties of LHPs, while keeping low environmental impacts and accessible costs of production. As an alternative, bismuth-based LFHPs have gained much attention due to their higher absorption coefficients, their more efficient charge transfer (compared to oxide perovskites), and their required thermodynamic potential for CO₂RR. However, despite all the remarkable advantages of bismuth halide perovskites, their use has been limited, owing to instability concerns. The performance of bismuth-based LFHPs are discussed, as well as stability strategies from intrinsic and extrinsic standpoints.

bismuth halide perovskites

CO₂RR

fuels

1. Introduction

Anthropogenic Carbon Dioxide (CO₂) is an exhaust gas that is mainly generated as a product of the fossil fuel combustion processes utilized to power the industrial, transport and domestic sectors. Its emission has high magnitude consequences on the atmosphere, as it is the main component of the greenhouse gases that lead to climate change. There is a continuous increase in the concentration of CO₂ in the atmosphere, which is driven by the high global electricity demand, estimated at approximately 1400 Terawatt-hours per year ^[1]. In 2021, the CO₂ emissions derived from the energy sector were 36.3 Gt, the highest annual quantity ever registered, caused by the sudden rebound from the global pandemic lockdown in 2020 ^[2]. Therefore, the pollution related to the increased CO₂ concentration in the atmosphere continues to be a matter of concern that requires action and global decision making.

Several solutions have been proposed to mitigate the environmental impact of the high CO₂ concentration in the atmosphere. The efforts have been diverse, and there are certain approaches that stand out. For instance, the

promulgation of environmental regulations focuses on carrying out preventive actions to avoid the emission of pollutants into the atmosphere. Another option to reduce CO₂ emissions is to improve the energy efficiency of the already-established fossil fuels, since this would result in a better use of these energetic resources [3][4]. Likewise, it is possible to use renewable fuels whose combustion reaction generates products with a lower environmental impact, e.g., natural gas, methanol, biogas, or alternative energy sources that do not involve the use of fossil fuels. However, these fuels are commonly obtained using nonrenewable and highly polluting fossil fuels. Alternatively, some technologies allow the use of CO₂ as a raw material in different processes to synthesize many industrial utility products (commodities) [5][6][7][8][9]. One of these processes is the production of short-chain hydrocarbons (solar fuels) through heterogeneous photocatalysis from CO₂ reduction [10][11][12][13][14][15]. This is one of the most promising technologies to help mitigate CO₂ pollution, since it can make use of sunlight to reduce CO₂, employing semiconductors and water. In this process, it is possible to capture and transform CO₂ into nonharmful products that, in some cases, can serve different purposes. The implementation of this technology at higher scales has been limited by the low efficiency of the photocatalysts. Nonetheless, materials with perovskite structure have been reported to exhibit outstanding efficiencies in the photocatalytic CO₂ Reduction Reaction (CO₂RR).

Scaling CO₂RR at pilot and industrial levels requires the design of photocatalyst materials with outstanding efficiencies and stabilities over extended periods. Other requirements may include chemical stability, low toxicity, high CO₂ conversion efficiency, high surface area, cost-effectiveness, accessibility, resistance to photocorrosion, and adequate redox potential to generate different solar fuels [8][10][16].

Inoue et al. were the first research group to report the photocatalytic CO₂RR using different photocatalysts (e.g., TiO₂, WO₃, ZnO, CdS, GaP, and SiC) suspended under UV-Visible irradiation [17], generating HCOOH, HCOH, CH₃OH, and CH₄ as reaction products. Some of these photocatalysts are still used for CO₂ reduction; however, to obtain higher efficiencies, it is necessary to implement certain modifications. These variations may include heterojunctions, anion functionalization, or encapsulation using porous materials [18][19][20][21][22].

Titanium dioxide (TiO₂) has been the most widely used photocatalyst since the earliest reports. It has many valuable properties: high photocatalytic activity, stability, inertness to chemical corrosion, and low toxicity. In addition, TiO₂ can perform CO₂RR to generate value-added products with good efficiencies. Despite this, it is often necessary to carry out the CO₂RR in unfavorable conditions, such as high pressures (up to 20 bar), an elevated temperature (>80 °C), and sacrificial agents [23]. Alternatively, other photocatalytic materials have also been utilized for CO₂RR with promising efficiencies. Some examples of these photocatalysts are scheelites AMO₄ (A = Ca, Sr, Ba) [24], AV₂O₆ (A = Ca, Sr, Ba) [25], rGO-CuO [26], Ti-MOF [27], Ni/BaTiO₃ [28], Cu/In₂O₃ [29], simple perovskites (ABO₃, A = Li, Na, K, B = Ta, Nb) [30][31], SrTiO₃ [32], LaCoO₃ [33], and more recently, metal halide perovskites ABX₃ (A = formamidinium, FA, methylammonium, MA, or Cs; B = Pb, Bi, or Sn; and X = Cl, Br or I) [34], which exhibit several promising features that have recently brought attention to their field of study.

2. Metal Halide Perovskites for CO₂RR

Perovskite structures are isostructural configurations to calcium titanate (CaTiO₃; a mineral commonly found in nature) and other cation variations (e.g., Ta or Nb). The general formula of perovskite materials is ABX₃, where A stands for organic or inorganic cations (e.g., MA⁺, FA⁺, NH₄⁺, K⁺, Sr²⁺, Ca²⁺, etc.) having larger radii than B (e.g., Ti⁴⁺, Bi³⁺, Pb²⁺, Ta⁴⁺, Nb⁴⁺, etc.) and X are anions, either oxides (O₂⁻) or halogens (I⁻, Br⁻, Cl⁻, or F⁻) [35][36][37]. In these structures, the central atom is not in direct contact with its neighboring coordination atoms, commonly giving these compounds the rare property of ferroelectricity [38] and other promising optoelectronic characteristics. Additionally, the use of organic ions on the A- and X-sites of perovskites leads to several geometric and structural degrees of freedom, which allows for detailed studies on the composition–structure–property relations of these materials [39]. Hydrogen bonds commonly assemble amino groups and halide ions in hybrid organic–inorganic perovskite structures; in which case, their ionic bonding facilitates their synthesis at low temperatures [40]. Among the different perovskite configurations, metal halides have stood out, since they exhibit remarkable properties for their use in the photocatalytic CO₂RR, such as:

(i) Ease of synthesis. These materials are distinguished by their low enthalpy of formation, which often grants them facile synthesis processes at normal temperatures (~25 °C) and pressures (~1 atm). Also, it allows for the formation of different morphologies with a high number of active sites [41][42].

(ii) Structure modulation. It has been demonstrated that metal halide perovskites can modulate their crystalline structures and energy bands by incorporating anions or cations from different groups [43][44][45][46]. In addition, the polarization refinement structure can induce an intensive internal electric field, which facilitates charge migration to the surface, improving the efficiency of CO₂RR [47]. On the other hand, the structure modulation can be carried out by variation of the morphology (e.g., bulk, nanoplates, nanorods, quantum dots, etc.) [48][49][50].

(iii) Light harvesting. The modulation of the composition of a halide perovskite can significantly alter its band gap, which can make it an excellent light harvester compared with other semiconductors. At an atomic level, the most common strategies for light-harvesting enhancement include extending the absorption range via band gap engineering, applying the plasmonic resonance enhancement effect, and the arrangement of light absorption using tandem absorber devices [51]. Recently, Jian et al. have proposed the formation of CsPbBr₃ nanocrystals with O-defective WO₃ composites as a solution for stable and highly efficient materials that can harvest the broadest solar spectrum possible [52]. This strategy increases CO₂RR efficiency up to 7-fold compared to pristine materials.

(iv) Exciton generation. The efficient generation of electron–hole pairs under excitation can enhance the photoconversion efficiency in CO₂RR and other applications, such as photovoltaics and photon detection [53]. This phenomenon is mainly seen in narrow-band perovskites, which can promote multiple exciton generation (MEG). Perovskite materials can exhibit a variety of exciton species under different excitation conditions, including biexciton and triple exciton [54]. The surface defects of perovskites are the main source of the production of charged excitons. Under weak light excitation, this is mostly generated by single exciton recombination; meanwhile, at medium excitation intensity, biexciton recombination is favored. On the other hand, by using strong light excitation, Auger recombination dominates the generation of charged excitons, and perovskite materials are mainly characterized by their recombination of these excitons. Lin et al. demonstrated that the decay time of single

excitons and biexcitons in Mn–CsPbBr₃ perovskites can be modified by applying an external magnetic field (300 mT), suppressing the recombination of the photogenerated charges and subsequently improving the efficiency of CO and CH₄ generation from CO₂RR [55].

(v) Long carrier diffusion lengths. Long carrier lifetime makes halide perovskite materials high-performance photovoltaic materials. Chen et al. proposed that the band-edge carrier lifetime increases when the system transitions from a lower rotational entropy to another phase with higher entropy [56]. These results suggest that the recombination of the photogenerated pair is inhibited by screening, leading to the formation of polarons and thereby extending their lifetime.

Moreover, there are several other factors that bolster the photovoltaic properties of metal halide perovskites, such as their high symmetry, the periodicity of their crystal structure (commonly referred to as 1D, 2D, or 3D perovskites), the arrangement of their polar organic cations, the ionic energy of their halides' anions, and the electronic configuration of the B-site cation of their structure [57]. These characteristics also increase their likelihood to obtain high photocatalytic yields [58]. More specifically, lead halide perovskites (LHP) have shown outstanding efficiencies for CO₂ photoreduction [59], owing to their narrow band gaps and adequate band structure suitable for conducting the photocatalytic CO₂RR. In addition, these materials have good charge transport properties [60], which allows charges to be efficiently separated and transferred within LHP band structure [61].

The general formula of LHPs is APbX₃, where A = organic and inorganic cations (e.g., Ca, K, Cs, Na, CH₃NH₃, or CH(NH₂)₂) and X = halides (e.g., I, Br, Cl, or F). Inorganic cations are preferable, as they are more stable [62]. The unit cell of the APbX₃ crystal lattice usually has a cubic geometry in which the Pb²⁺ cation is in the center of the octahedra, coordinating with six X anions to form [BX₆]⁴⁻ ions, while the A-site cation is located at the vertices. Of these materials, CsPbBr₃ perovskites have a particularly high photocatalytic performance for CO₂ photoreduction [59][63][64], as well as high stability, even in ten consecutive cycles of CO₂RR evaluation [65].

Despite the promising activity of LHPs, the presence of lead in their structure could generate environmental toxicity problems. Therefore, various efforts have been made to replace this metal without sacrificing its superior performance, leading to the development of lead-free halide perovskites (LFHP). One of the most frequent ones is the alteration of the periodicity in the crystalline arrangement of LHP materials, which is achieved by modifying their layers to optimize their optical properties [66]. For this purpose, different synthesis methods have been developed using various reactants, solvents, and ligands that allow for the obtention of desired optical properties in these materials and a high environmental stability [67]. As a result, many elements with different oxidation states have been used to form various perovskite structures, as shown in **Figure 1**.

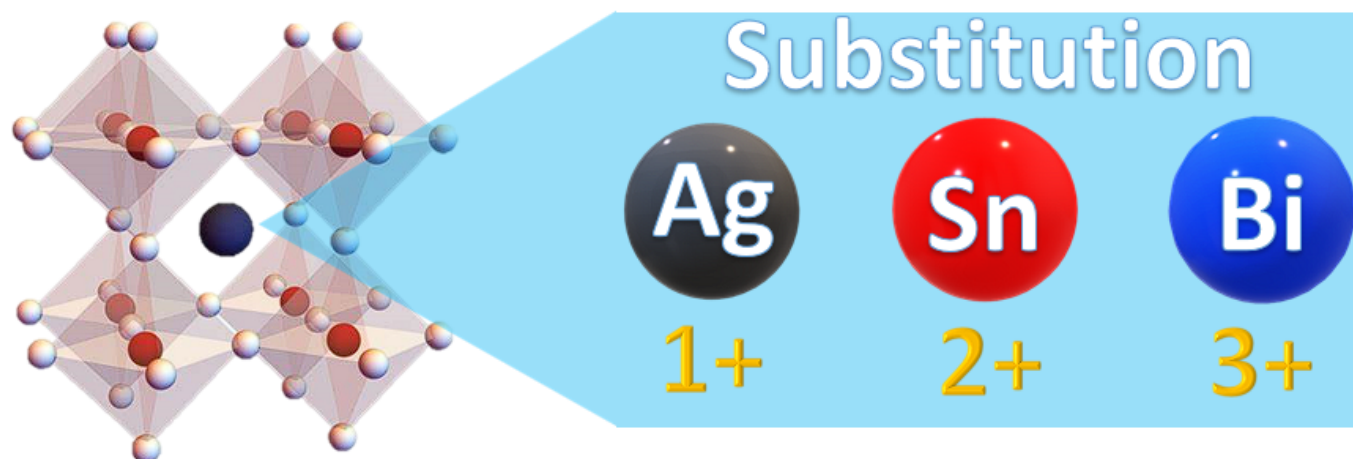


Figure 1. Substitution of Pb in Lead Halide Perovskites.

Different families of chemical elements can form LFHP structures, such as some transition metals (Pd [68], Cd [69]), chalcogenides (Zr, Hf) [70], and La [71]. There is also great potential in replacing Pb with group 14 metals; however, Sn²⁺ and Ge²⁺ cations tend to undergo oxidation due to the high-energy 5s orbitals that promote a highly unstable structure at ambient exposure [72]. There are also reports on the use of mixed or trivalent cations to form structures of the A₃B₂X₉ or A₂B⁺B³⁺X₆ types. Alternatively, Bi³⁺ and Sb³⁺ ions are promising candidates to replace Pb²⁺ and develop stable, lead-free perovskites. In some cases, these structures exhibit low-dimensional A₃M(III)₂X₉ structures whose properties have not been extensively studied, especially in photocatalytic CO₂RR. To substitute Pb and form stable perovskite materials, the size of the A, B, and X ions should satisfy the Goldschmidt tolerance factor (*t*), as shown in Equation (1):

$$t = \frac{r_A + r_X}{\sqrt{2}(r_B + r_x)} \quad (1)$$

In this equation, variables r_A , r_B , and r_X are the ionic radii of each element in the ABX₃ structure [73]. The perovskite materials show good stability when the tolerance factor is equal or close to one.

3. Bismuth Halide Perovskites

In the case of LFHPs, bismuth has a similar ionic radius to lead, as well as comparable properties to substitute this atom. Thus, the tolerance factor rule is satisfied, and the stability of the Bi-based perovskite materials can theoretically be enhanced when this substitution takes place. Bismuth provides an attractive option due to its nontoxic nature and chemical stability [74]. Its trivalent (3+) oxidation state causes materials to form an A₃Bi₂X₉ structure, where A can be K⁺, Rb⁺, Cs⁺, or methylammonium MA⁺, and X can be I, Br, or Cl. Moreover, it was found that Bi-based perovskite materials possess a higher absorption coefficient, which renders them an efficient light-absorbing material for solar cell applications and, recently, for photocatalytic applications [73][75][76][77][78][79]. There

are also reports on the use of Cs₃Bi₂I₆Br₃ films as solar cells, for which the highest power conversion efficiency (PCE) reported so far was 1.15% [75]. In addition, bismuth halides have been demonstrated to be good candidates for oxidizing a variety of organic compounds, such as thiamazole [76], vanillyl alcohol [77], rhodamine B [78], phenol [79], etc.

So far, most of the reports related to CO₂RR using Bismuth Halide Perovskites employ Cs⁺ as the A-site cation in the A₃Bi₂X₉ (X= I, Cl, Br, F) configuration. The best result for CO generation for these perovskites was obtained via the design of a Cs₃Bi₂I₉-CeO₂ heterostructure (135 μmol g⁻¹ [80]), whereas the implementation of three stability strategies such as encapsulation, structure reconfiguration, and heterostructure design allowed for the highest efficiency to produce CH₄ (151 μmol g⁻¹ [81]). Both efficiencies (higher than other traditional and LHP perovskites) demonstrated the feasibility of using CO₂RR to generate clean and renewable solar fuels, and these results were often attributed to a more efficient charge transfer with longer lifetimes, which grants more free charges for CO₂RR.

Even with these remarkable findings, it is well-known that the low stability of Bismuth Halide Perovskites in ambient conditions hinders their commercialization and upscaling to the industrial level. Hence the lack of evidence regarding the recycling of these materials in consecutive cycles of evaluation, only reporting 5 h to 21 days of stability in gas–solid reactions. Some of the most common reasons for low stability in perovskites are shown in **Figure 2**.

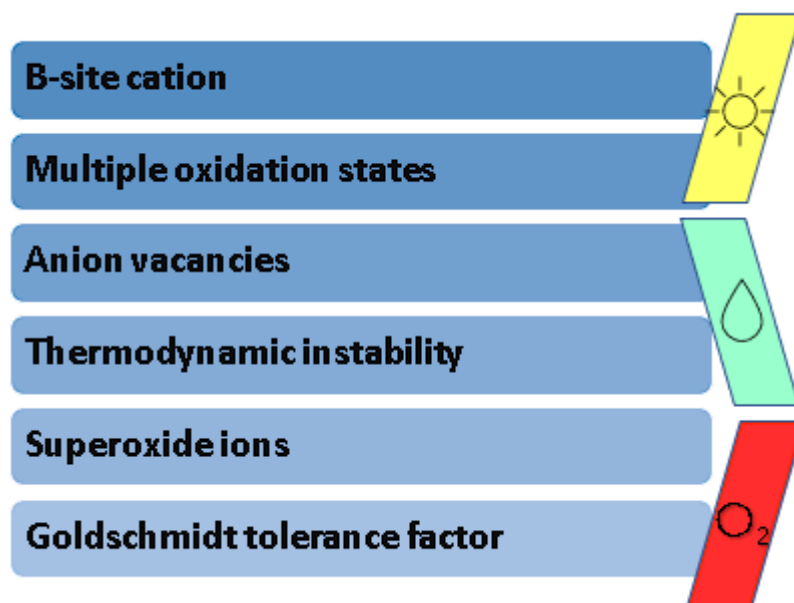


Figure 2. Factors that hinder perovskite stability.

In the research of stable perovskite photocatalysts, there are concerns regarding several factors that lead to instability, such as: (i) the B-site cation in the perovskite A₃B₂X₉ configuration, as it must possess a good compatibility with this structure; (ii) the oxidation states of the ions that conform said structure, which determine the spontaneity with which these can undergo reduction or oxidation processes and lead to instability; (iii) anion

vacancies, as these are inherent defects present in the perovskite structure that cause its degradation; (iv) thermodynamic instability, since the energetic feasibility that allows perovskites to be synthesized at room temperatures can also signify that these materials are prone to dissociate with the same ease; (v) the formation of superoxide ions, which are derived from the excitation of irradiated perovskites in the presence of atmospheric oxygen; and (vi) the aforementioned Goldschmidt tolerance factor, as it is an accurate indicator of the stability of a theoretical perovskite structure. Considering these aspects, several authors have proposed different strategies to increase the stability of halide perovskites.

4. Stability of Bismuth Halide Perovskites

The strategies with which the stability of photocatalysts can be improved are classified into two main approaches: intrinsic and extrinsic, depending on the nature of the employed methodology.

4.1 Intrinsic approach

This approach is widely used to improve the stability of metal halide perovskites through structural modification, which involves the alteration of the composition of cations and anions that are inherent to the perovskite structure [82][83]. The formation of solid solutions and double perovskites are examples of this approach. Likewise, the obtention of low-dimensional-networked perovskites promotes the formation of more stable crystal structures by selecting appropriate manufacturing techniques. Stoichiometry modification then settles the network in a quasi-zero-dimensional (0D) configuration, where the metal halide octahedra are almost isolated [84]. Another successfully intrinsic strategy is passivation [85]. This strategy allows the removal of dangling bonds, which act as recombination centers associated with defects, promoting better stability and optical properties. Antisolvent engineering is another strategy that speeds up nucleation during perovskite synthesis through solvent extraction [86][87][88]. This strategy allows the obtention of dense, high-quality films of bismuth halide perovskites with enhanced stability.

4.2 Extrinsic approach

This approach is characterized by the modification of the perovskite's external properties without altering its internal composition. Among these strategies, encapsulation is one of the most used. It consists of the coverage of the perovskite to prevent exposure to moisture, oxygen, UV light, and temperature, thus protecting the structure. The encapsulation can be done by glass–glass covering of the edges of the substrate with an adhesive, as well as the deposition of a polymer coating. The adhesives can be ethylene methacrylate (EMA), ethylene vinyl acetate (EVA), polyisobutylene (PIB), and epoxy resins activated with UV light [89]. Alternatively, encapsulation can be done by depositing polymer coatings, e.g., polyethylene oxide, polyvinyl pyridine. The construction of heterostructures or Z-schemes between perovskites and other semiconductors has contributed to the design of promising stabilities for photocatalytic reactions since electrons are not available to react with the adsorbed oxygen. This avoids the degradation of the perovskite structure [90][91][92]. Another option is the dispersion of the perovskite nanoparticles in porous support for enhanced electron and hole separation, more accessible active sites, and close contact with the

reaction species [42]. At the same time, adding adequate reactants to the medium can promote good stability of the perovskite structure. For example, it has been proved that the addition of HI during the evaluation of MA₃Bi₂I₉ promotes excellent phase stability and enhanced photocatalytic activity for H₂ evolution [93].

Some of these strategies have been implemented in bismuth halide perovskites to achieve better stabilities and efficiencies in photocatalytic CO₂RR, mainly for Cs₃Bi₂X₉ perovskites. So far, the stability of the Cs₃Bi₂X₉ perovskite has been boosted by implementing two intrinsic strategies: solid solutions [94] and double perovskites [95]; as well as two extrinsic methodologies: the formation of heterojunctions with other semiconductors [96] and the encapsulation of the perovskites in porous supports [97]. The strategies implemented for the stable performance of bismuth halide perovskite photocatalysts are summarized in **Figure 3**.

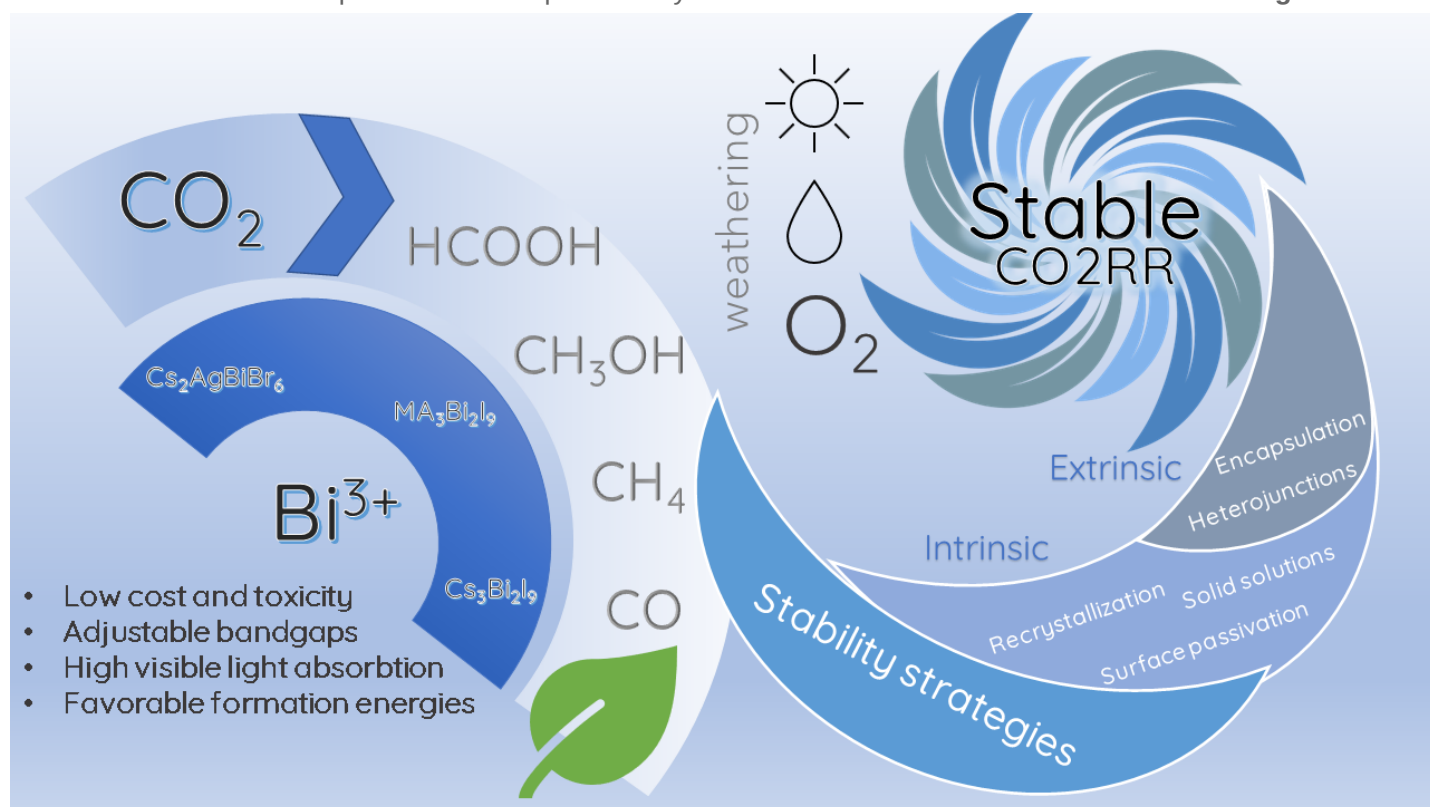


Figure 3. Strategies in bismuth halide perovskite for a stable CO₂RR.

References

1. IEA. Global Energy Review: CO₂ Emissions in 2021—Analysis. 2021. Available online: <https://www.iea.org/reports/global-energy-review-co2-emissions-in-2021-2> (accessed on 1 September 2022).
2. Energy Agency, I. Global Energy Review: CO₂ Emissions in 2021 Global Emissions Rebound Sharply to Highest Ever Level. 2021. Available online: www.iea.org/t&c/ (accessed on 1 September 2022).

3. Ponce, P.; Khan, S.A.R. A causal link between renewable energy, energy efficiency, property rights, and CO₂ emissions in developed countries: A road map for environmental sustainability. *Environ. Sci. Pollut. Res.* 2021, 28, 37804–37817.
4. Answer, M.K.; Iqbal, W.; Ahmad, U.S.; Fatima, A.; Chaudhry, I.S. Environmental efficiency and the role of energy innovation in emissions reduction. *Environ. Sci. Pollut. Res.* 2020, 27, 29451–29463.
5. Salehizadeh, H.; Yan, N.; Farnood, R. Recent advances in microbial CO₂ fixation and conversion to value-added products. *Chem. Eng. J.* 2020, 390, 124584.
6. Meunier, N.; Chauvy, R.; Mouhoubi, S.; Thomas, D.; De Weireld, G. Alternative production of methanol from industrial CO₂. *Renew. Energy* 2020, 146, 1192–1203.
7. Kumaravel, V.; Bartlett, J.; Pillai, S.C. Photoelectrochemical Conversion of Carbon Dioxide (CO₂) into Fuels and Value-Added Products. *ACS Energy Lett.* 2020, 5, 486–519.
8. Garba, M.D.; Usman, M.; Khan, S.; Shehzad, F.; Galadima, A.; Ehsan, M.F.; Ghanem, A.S.; Humayun, M. CO₂ towards fuels: A review of catalytic conversion of carbon dioxide to hydrocarbons. *J. Environ. Chem. Eng.* 2021, 9, 104756.
9. Mustafa, A.; Lougou, B.G.; Shuai, Y.; Wang, Z.; Tan, H. Current technology development for CO₂ utilization into solar fuels and chemicals: A review. *J. Energy Chem.* 2020, 9, 96–123.
10. Gong, E.; Ali, S.; Hiragond, C.B.; Kim, H.S.; Powar, N.S.; Kim, D.; Kim, H.; In, S.-I. Solar fuels: Research and development strategies to accelerate photocatalytic CO₂ conversion into hydrocarbon fuels. *Energy Environ. Sci.* 2022, 15, 880–893.
11. Patial, S.; Kumar, R.; Raizada, P.; Singh, P.; Le, Q.V.; Lichtfouse, E.; Nguyen, D.L.T.; Nguyen, V.-H. Boosting light-driven CO₂ reduction into solar fuels: Mainstream avenues for engineering ZnO-based photocatalysts. *Environ. Res.* 2021, 197, 111134.
12. Omr, H.A.E.; Horn, M.W.; Lee, H. Low-Dimensional Nanostructured Photocatalysts for Efficient CO₂ Conversion into Solar Fuels. *Catalysts* 2021, 11, 418.
13. Shen, Y.; Han, Q.; Hu, J.; Gao, W.; Wang, L.; Yang, L.; Gao, C.; Shen, Q.; Wu, C.; Wang, X.; et al. Artificial Trees for Artificial Photosynthesis: Construction of Dendrite-Structured α -Fe₂O₃/g-C₃N₄ Z-Scheme System for Efficient CO₂ Reduction into Solar Fuels. *ACS Appl. Energy Mater.* 2020, 3, 6561–6572.
14. Burke, R.; Bren, K.L.; Krauss, T.D. Semiconductor nanocrystal photocatalysis for the production of solar fuels. *J. Chem. Phys.* 2021, 154, 030901.
15. Xia, Y.; Zhang, L.; Hu, B.; Yu, J.; Al-Ghamdi, A.A.; Wageh, S. Design of highly-active photocatalytic materials for solar fuel production. *Chem. Eng. J.* 2021, 421, 127732.

16. Ma, Z.; Wang, Y.; Lu, Y.; Ning, H.; Zhang, J. Tackling Challenges in Perovskite-Type Metal Oxide Photocatalysts. *Energy Technol.* 2021, 9, 2001019.
17. Inoue, T.; Fujishima, A.; Konishi, S.; Honda, K. Photoelectrocatalytic reduction of carbon dioxide in aqueous suspensions of semiconductor powders. *Nature* 1979, 277, 637–638.
18. Kamal, K.M.; Narayan, R.; Chandran, N.; Popović, S.; Nazrulla, M.A.; Kovač, J.; Vrtovec, N.; Bele, M.; Hodnik, N.; Likozar, M.M.K.B. Synergistic enhancement of photocatalytic CO₂ reduction by plasmonic Au nanoparticles on TiO₂ decorated N-graphene heterostructure catalyst for high selectivity methane production. *Appl. Catal. B Environ.* 2022, 307, 121181.
19. Tahir, B.; Tahir, M.; Ghazali, M.; Nawawi, M. Highly stable 3D/2D WO₃/g-C₃N₄ Z-scheme heterojunction for stimulating photocatalytic CO₂ reduction by H₂O/H₂ to CO and CH₄ under visible light. *J. CO₂ Util.* 2020, 41, 101270.
20. Deng, H.; Xu, F.; Cheng, B.; Yu, J.; Ho, W. Photocatalytic CO₂ reduction of C/ZnO nanofibers enhanced by an Ni-NiS cocatalyst. *Nanoscale* 2020, 12, 7206–7213.
21. Wang, S.; Wang, X. Photocatalytic CO₂ reduction by CdS promoted with a zeolitic imidazolate framework. *Appl. Catal. B Environ.* 2015, 162, 494–500.
22. Xiao, S.; Guan, Y.; Shang, H.; Li, H.; Tian, Z.; Liu, S.; Chen, W.; Yang, J. An S-scheme NH₂-UiO-66/SiC photocatalyst via microwave synthesis with improved CO₂ reduction activity. *J. CO₂ Util.* 2022, 55, 101806.
23. Galli, F.; Compagnoni, M.; Vitali, D.; Pirola, C.; Bianchi, C.L.; Villa, A.; Prati, L.; Rossetti, I. CO₂ photoreduction at high pressure to both gas and liquid products over titanium dioxide, *Appl. Catal. B Environ.* 2017, 200, 386–391.
24. Luévano-Hipólito, E.; Torres-Martínez, L.M. Ink-jet printing films of molybdates of alkaline earth metals with scheelite structure applied in the photocatalytic CO₂ reduction. *J. Photochem. Photobiol. A Chem.* 2019, 368, 15–22.
25. Aguirre-Astrain, A.; Luévano-Hipólito, E.; Torres-Martínez, L.M. Integration of 2D printing technologies for AV₂O₆ (A=Ca, Sr, Ba)-MO (M=Cu, Ni, Zn) photocatalyst manufacturing to solar fuels production using seawater. *Int. J. Hydrog. Energy* 2021, 46, 37294–37310.
26. Gusain, R.; Kumar, P.; Sharma, O.P.; Jain, S.L.; Khatri, O.P. Reduced graphene oxide–CuO nanocomposites for photocatalytic conversion of CO₂ into methanol under visible light irradiation. *Appl. Catal. B Environ.* 2016, 181, 352–362.
27. Wang, S.; Cabrero-Antonino, M.; Navalón, S.; Cao, C.-c.; Tissot, A.; Dovgaliuk, I.; Marrot, J.; Martineau-Corcós, C.; Yu, L.; Wang, H.; et al. A Robust Titanium Isophthalate Metal-Organic Framework for Visible-Light Photocatalytic CO₂ Methanation. *Chem* 2020, 6, 3409–3427.

28. Mateo, D.; Morlanes, N.; Maity, P.; Shterk, G.; Mohammed, O.F.; Gascon, J. Efficient Visible-Light Driven Photothermal Conversion of CO₂ to Methane by Nickel Nanoparticles. *Adv. Funct. Mater.* 2021, 31, 2008244.
29. Wang, X.; Ng, D.; Du, H.; Hornung, C.H.; Polyzos, A.; Seeber, A.; Li, H.; Huo, Y.; Xie, Z. Copper decorated indium oxide rods for photocatalytic CO₂ conversion under simulated sun light. *J. CO₂ Util.* 2022, 58, 101909.
30. Luévano-Hipólito, E.; Torres-Martínez, L.M. CO₂ photoreduction with H₂O to C₁ and C₂ products over perovskite films of alkaline niobates ANbO₃ (A = Li, Na, K). *Fuel* 2022, 320, 123934.
31. Teramura, K.; Okuoka, S.; Tsuneoka, H.; Shishido, T.; Tanaka, T. Photocatalytic reduction of CO₂ using H₂ as reductant over ATaO₃ photocatalysts (A = Li, Na, K). *Appl. Catal. B.* 2010, 96, 565–568.
32. Luo, C.; Zhao, J.; Li, Y.; Zhao, W.; Zeng, Y.; Wang, C. Photocatalytic CO₂ reduction over SrTiO₃: Correlation between surface structure and activity. *Appl. Surf. Sci.* 2018, 447, 627–635.
33. Qin, J.; Lin, L.; Wang, X. A perovskite oxide LaCoO₃ cocatalyst for efficient photocatalytic reduction of CO₂ with visible light. *ChemComm* 2018, 54, 2272–2275.
34. Raza, M.A.; Li, F.; Que, M.; Zhu, L.; Chen, X. Photocatalytic reduction of CO₂ by halide perovskites: Recent advances and future perspectives. *Mater. Adv.* 2021, 2, 7187–7209.
35. Manikandan, A.; Slimani, Y.; Dinesh, A.; Khan, A.; Thanrasu, K.; Baykal, A.; Jaganathan, S.K.; Dzudzevic-Cancari, H.; Asirid, A.M. Perovskite's potential functionality in a composite structure. In *Hybrid Perovskite Composite Materials: Design to Applications*; Woodhead Publishing: Cambridge, UK, 2021; Volume 1, pp. 181–202.
36. Brittman, S.; Adhyaksa, G.W.P.; Garnett, E.C. The expanding world of hybrid perovskites: Materials properties and emerging applications. *MRS Commun.* 2015, 5, 7–26.
37. Gao, P.; Grätzel, M.; Nazeeruddin, M.K. Organohalide Lead Perovskites for Photovoltaic Applications. *Energy Environ. Sci.* 2014, 7, 2448–2463.
38. Shahrokhi, S.; Gao, W.; Wang, Y.; Anandan, P.R.; Rahaman, M.Z.; Singh, S.; Wang, D.; Cazorla, C.; Yuan, G.; Liu, J.-M.; et al. Emergence of ferroelectricity in halide perovskites. *Small Methods* 2020, 4, 2000149.
39. Burger, S.; Grover, S.; Butler, K.T.; Boström, H.L.; Grau-Crespo, R.; Kieslich, G. Tilt and shift polymorphism in molecular perovskites. *Mater Horizon.* 2021, 8, 2444–2450.
40. Dong, Y.; Zhao, Y.; Zhang, S.; Dai, Y.; Liu, L.; Li, Y.; Chen, Q. Recent advances toward practical use of halide perovskite nanocrystals. *J. Mater. Chem. A* 2018, 6, 21729–21746.
41. Sanders, S.; Stümmler, D.; Pfeiffer, P.; Ackermann, N.; Schimkat, F.; Simkus, G.; Heuken, M.; Baumann, P.K.; Vescan, A.; Kalisch, H. Morphology Control of Organic–Inorganic Bismuth-Based

- Perovskites for Solar Cell Application. *Phys. Status. Solidi A* 2018, 215, 1800409.
42. Dai, Y.; Poidevin, C.; Ochoa-Hernández, C.; Auer, A.A.; Tüysüz, H. A Supported Bismuth Halide Perovskite Photocatalyst for Selective Aliphatic and Aromatic C–H Bond Activation. *Angew. Chem.* 2020, 59, 5788–5796.
 43. Jin, S. Can We Find the Perfect A-Cations for Halide Perovskites? *ACS Energy Lett.* 2021, 6, 3386–3389.
 44. Tao, J.; Liu, X.; Shen, J.; Han, S.; Guan, L.; Fu, G.; Kuang, D.-B.; Yang, S. F-Type Pseudo-Halide Anions for High-Efficiency and Stable Wide-Band-Gap Inverted Perovskite Solar Cells with Fill Factor Exceeding 84%. *ACS Nano* 2022, 16, 10798–10810.
 45. Sun, X.; Ji, L.Y.; Chen, W.W.; Guo, X.; Wang, H.H.; Lei, M.; Wang, Q.; Li, Y.F. Halide anion–fullerene π noncovalent interactions: N-doping and a halide anion migration mechanism in p–i–n perovskite solar cells. *J. Mater. Chem.* 2017, 5, 20720–20728.
 46. Wang, Y.; Zhang, X.; Wang, D.; Li, X.; Meng, J.; You, J.; Yin, Z.; Wu, J. Compositional Engineering of Mixed-Cation Lead Mixed-Halide Perovskites for High-Performance Photodetectors. *ACS Appl. Mater. Interfaces* 2019, 11, 28005–28012.
 47. Yu, Z.; Yang, K.; Yu, C.; Lu, K.; Huang, W.; Xu, L.; Zou, L.; Wang, S.; Chen, Z.; Hu, J.; et al. Steering Unit Cell Dipole and Internal Electric Field by Highly Dispersed Er atoms Embedded into NiO for Efficient CO₂ Photoreduction. *Adv. Funct. Mater.* 2022, 32, 2111999.
 48. Liu, X.; Zhang, Z.; Lin, F.; Cheng, Y. Structural modulation and assembling of metal halide perovskites for solar cells and light-emitting diodes. *InfoMat* 2021, 3, 1218–1250.
 49. Guan, X.; Lei, Z.; Yu, X.; Lin, C.-H.; Huang, J.-K.; Huang, C.-Y.; Feng, L.; Ajayan Vinu, L.; Yi, J.; Wu, T. Low-Dimensional Metal-Halide Perovskites as High-Performance Materials for Memory Applications. *Small* 2022, 18, 2203311.
 50. Ling, X.; Yuan, J.; Ma, W. The Rise of Colloidal Lead Halide Perovskite Quantum Dot Solar Cells. *Acc. Mater. Res.* 2022, 8, 866–878.
 51. Levchuk, I.; Osvet, A.; Tang, X.; Brandl, M.; Perea, J.D.; Hoegl, F.; Matt, G.J.; Hock, R.; Batentschuk, M.; Brabec, C.J. Brightly luminescent and color-tunable formamidinium lead halide perovskite FAPbX (X = Cl, Br, I) colloidal nanocrystals. *Nano Lett.* 2017, 17, 2765–2770.
 52. Jiang, X.; Ding, Y.; Zheng, S.; Ye, Y.; Li, Z.; Xu, L.; Wang, J.; Li, Z.; Loh, X.J.; Ye, E.; et al. In-Situ Generated CsPbBr₃ Nanocrystals on O-Defective WO₃ for Photocatalytic CO₂ Reduction. *ChemSusChem* 2021, 15, e202102295.
 53. Chen, Y.; Yin, J.; Wei, Q.; Wang, C.; Wang, X.; Ren, H.; Yu, S.F.; Bakr, O.M.; Mohammed, O.F.; Li, M. Multiple exciton generation in tin–lead halide perovskite nanocrystals for photocurrent quantum efficiency enhancement. *Nat. Photon.* 2022, 16, 485–490.

54. Gao, W.; Ding, J.; Bai, Z.; Qi, Y.; Wang, Y.; Lv, Z. Multiple excitons dynamics of lead halide perovskite. *Nanophotonics* 2021, 10, 3945–3955.
55. Lin, C.-C.; Liu, T.-R.; Lin, S.-R.; Boopathi, K.M.; Chiang, C.-H.; Tzeng, W.-Y.; Chien, W.-H.C.; Hsu, H.-S.; Luo, C.-W.; Tsai, H.-Y.; et al. Spin-Polarized Photocatalytic CO₂ Reduction of Mn-Doped Perovskite Nanoplates. *J. Am. Chem. Soc.* 2022, 144, 15718–15726.
56. Chen, T.; Chen, W.-L.; Foley, B.J.; Lee, S.-H. Origin of long lifetime of band-edge charge carriers in organic–inorganic lead iodide perovskites. *Appl. Phys. Sci.* 2017, 114, 7519–7524.
57. Meyer, E.; Mutukwa, D.; Zingwe, N.; Taziwa, R. Lead-free halide double perovskites: A review of the structural, optical, and stability properties as well as their viability to replace lead halide perovskites. *Metals* 2018, 8, 667.
58. Han, C.; Zhu, X.; San Martin, J.; Lin, Y.; Spears, S.; Yan, Y. Recent Progress in Engineering Metal Halide Perovskites for Efficient Visible-Light-Driven Photocatalysis. *ChemSusChem* 2020, 13, 4005–4025.
59. Wang, J.; Wang, J.; Li, N.; Du, X.; Ma, J.; He, C.; Li, Z. Direct Z scheme 0D/2D heterojunction of CsPbBr₃ quantum dots/Bi₂WO₆ nanosheets for efficient photocatalytic CO₂ reduction. *ACS Appl. Mater. Interfaces* 2020, 12, 31477–31485.
60. Jin, Z.; Zhang, Z.; Xiu, J.; Song, H.; Gatti, T.; He, Z. A critical review on bismuth and antimony halide based perovskites and their derivatives for photovoltaic applications: Recent advances and challenges. *J. Mater. Chem. A* 2020, 8, 16166–16188.
61. Liao, J.-F.; Cai, Y.-T.; Li, J.-Y.; Jiang, Y.; Wang, X.-D.; Chen, H.-Y.; Kuang, D.-B. Plasmonic CsPbBr₃–Au nanocomposite for excitation wavelength dependent photocatalytic CO₂ reduction. *J. Energy Chem.* 2021, 53, 309–315.
62. Fan, Q.; Biesold-McGee, G.V.; Ma, J.; Xu, Q.; Pan, S.; Peng, J.; Lin, Z. Lead-free halide perovskite nanocrystals: Crystal structures, synthesis, stabilities, and optical properties. *Angew Chem. Int. Ed.* 2020, 59, 1030–1046.
63. Chen, Z.; Hu, Y.; Wang, J.; Shen, Q.; Zhang, Y.; Ding, C.; Bai, Y.; Jiang, G.; Li, Z.; Gaponik, N. Boosting photocatalytic CO₂ reduction on CsPbBr₃ perovskite nanocrystals by immobilizing metal complexes. *Chem. Mater.* 2020, 32, 1517–1525.
64. Ou, M.; Tu, W.; Yin, S.; Xing, W.; Wu, S.; Wang, H.; Wan, S.; Zhong, Q.; Xu, R. Amino-assisted anchoring of CsPbBr₃ perovskite quantum dots on porous g-C₃N₄ for enhanced photocatalytic CO₂ reduction. *Angew. Chem.* 2018, 57, 13570–13574.
65. Wang, X.; He, J.; Li, J.; Lu, G.; Dong, F.; Majima, T.; Zhu, M. Immobilizing perovskite CsPbBr₃ nanocrystals on Black phosphorus nanosheets for boosting charge separation and photocatalytic CO₂ reduction. *Appl. Catal. B.* 2020, 277, 119230.

66. Connor, B.A.; Leppert, L.; Smith, M.D.; Neaton, J.B.; Karunadasa, H.I. Layered halide double perovskites: Dimensional reduction of Cs₂AgBiBr₆. *J. Am. Chem. Soc.* 2018, 140, 5235–5240.
67. Brandt, R.E.; Stevanović, V.; Ginley, D.S.; Buonassisi, T. Identifying defect-tolerant semiconductors with high minority-carrier lifetimes: Beyond hybrid lead halide perovskites. *MRS Commun.* 2015, 5, 265–275.
68. Huang, S.; Shan, H.; Xuan, W.; Xu, W.; Hu, D.; Zhu, L.; Huang, C.; Sui, W.; Xiao, C.; Zhao, Y.; et al. High-Performance Humidity Sensor Based on CsPdBr₃ Nanocrystals for Noncontact Sensing of Hydromechanical Characteristics of Unsaturated Soil. *Phys. Status Solidi–Rapid Res. Lett.* 2022, 16, 2200017.
69. Guo, J.; Hu, Q.; Lu, M.; Li, A.; Zhang, X.; Sheng, R.; Chen, P.; Zhang, Y.; Wu, J.; Fu, Y.; et al. Pb²⁺ doped CsCdBr₃ perovskite nanorods for pure-blue light-emitting diodes. *Chem. Eng. J.* 2022, 427, 131010.
70. Chaiyawat, K.; Laosiritaworn, Y.; Jaroenjittichai, A.P. First-principles study on structural stability and reaction with H₂O and O₂ of vacancy-ordered double perovskite halides: Cs₂(Ti, Zr, Hf)X₆. *Results Phys.* 2021, 25, 104225.
71. Gundiah, G.; Brennan, K.; Yan, Z.; Samulon, E.C.; Wu, G.; Bizarri, G.A.; Derenzo, S.E.; Bourret-Courchesne, E.D. Structure and scintillation properties of Ce³⁺-activated Cs₂NaLaCl₆, Cs₃LaCl₆, Cs₂NaLaBr₆, Cs₃LaBr₆, Cs₂NaLaI₆ and Cs₃LaI₆. *J. Lumin.* 2014, 149, 374–384.
72. Krishnamoorthy, T.; Ding, H.; Yan, C.; Leong, W.L.; Baikie, T.; Zhang, Z.; Sherburne, M.; Li, S.; Asta, M.; Mathews, N.; et al. Lead-free germanium iodide perovskite materials for photovoltaic applications. *J. Mater. Chem. A* 2015, 3, 23829.
73. Ahmad, K. Bismuth Halide Perovskites for Photovoltaic Applications. In *Bismuth—Fundamentals and Optoelectronic Applications*; IntechOpen: London, UK, 2020.
74. Bhosale, S.S.; Kharade, A.K.; Jokar, E.; Fathi, A.; Chang, S.-m.; Diao, E.W.-G. Mechanism of Photocatalytic CO₂ Reduction by Bismuth-Based Perovskite Nanocrystals at the Gas–Solid Interface. *J. Am. Chem. Soc.* 2019, 141, 20434–20442.
75. Yu, B.-B.; Liao, M.; Yang, J.; Chen, W.; Zhu, Y.; Zhang, X.; Duan, T.; Yao, W.; Wei, S.-H.; He, Z. Alloy-induced phase transition and enhanced photovoltaic performance: The case of Cs₃Bi₂I_{9–x}Br_x perovskite solar cells. *J. Mater. Sci.* 2019, 7, 8818–8825.
76. Cui, Z.; Wu, Y.; Zhang, S.; Fu, H.; Chen, G.; Lou, Z.; Liu, X.; Zhang, Q.; Wang, Z.; Zheng, Z.; et al. Insight into a strategy to improve charge carrier migration in lead-free bismuth-based halide perovskite for efficient selective oxidation of thioanisole under visible light. *Chem. Eng. J.* 2023, 451, 138927.
77. Estrada-Pomares, J.; Ramos-Terrón, S.; Lasarte-Aragonés, G.; Lucena, R.; Cárdenas, S.; Rodríguez-Padrón, D.; Luque, R.; de Miguel, G. Mechanochemically designed bismuth-based

- halide perovskites for efficient photocatalytic oxidation of vanillyl alcohol. *J. Mater. Chem. A* 2022, 10, 11298–11305.
78. Bresolin, B.-M.; Günnemann, C.; Bahnemann, D.W.; Sillanpää, M. Pb-Free Cs₃Bi₂I₉ Perovskite as a Visible-Light-Active Photocatalyst for Organic Pollutant Degradation. *Nanomaterials* 2020, 10, 763.
79. Miodyńska, M.; Mikolajczyk, A.; Mazierski, P.; Klimczuk, T.; Lisowski, W.; Trykowski, G.; Zaleska-Medynska, A. Lead-free bismuth-based perovskites coupled with g-C₃N₄: A machine learning based novel approach for visible light induced degradation of pollutants. *Appl. Surf. Sci.* 2022, 588, 152921.
80. Feng, Y.-X.; Dong, G.-X.; Su, K.; Liu, Z.-L.; Zhang, W.; Zhang, M.; Lu, T.-B. Self-template-oriented synthesis of lead-free perovskite Cs₃Bi₂I₉ nanosheets for boosting photocatalysis of CO₂ reduction over Z-scheme heterojunction Cs₃Bi₂I₉/CeO₂. *J. Energy Chem.* 2022, 69, 348–355.
81. Sun, Q.-M.; Xu, J.-J.; Tao, F.-F.; Ye, W.; Zhou, C.; He, J.-H.; Lu, J.-M. Boosted Inner Surface Charge Transfer in Perovskite Titania Frameworks for Efficient and Selective Photocatalytic CO₂ Reduction to Methane. *Angew. Chem.* 2022, 134, e202200872.
82. Song, W.; Zhang, X.; Lammar, S.; Qiu, W.; Kuang, Y.; Ruttens, B.; D'Haen, J.; Vaesen, I.; Conard, T.; Abdulraheem, Y.; et al. Critical Role of Perovskite Film Stoichiometry in Determining Solar Cell Operational Stability: A Study on the Effects of Volatile A-Cation Additives. *ACS Appl. Mater. Interfaces* 2022, 14, 27922–27931.
83. Fabian, D.M.; Ganose, A.M.; Ziller, J.W.; Scanlon, D.O.; Beard, M.C.; Ardo, S. Influence of One Specific Carbon–Carbon Bond on the Quality, Stability, and Photovoltaic Performance of Hybrid Organic–Inorganic Bismuth Iodide Materials. *ACS Appl. Energy Mater.* 2019, 2, 1579–1587.
84. Trifiletti, V.; Luong, S.; Tseberlidis, G.; Riva, S.; Galindez, E.S.S.; Gillin, W.P.; Binetti, S.; Fenwick, O. Two-Step Synthesis of Bismuth-Based Hybrid Halide Perovskite Thin-Films. *Materials* 2021, 14, 7827.
85. Leng, M.; Yang, Y.; Chen, Z.; Gao, W.; Zhang, J.; Niu, G.; Li, D.; Song, H.; Zhang, J.; Jin, S.; et al. Surface Passivation of Bismuth-Based Perovskite Variant Quantum Dots to Achieve Efficient Blue Emission. *Nano Lett.* 2018, 18, 6076–6083.
86. Mali, S.S.; Kim, H.; Kim, D.-H.; Hong, C.K. Anti-Solvent Assisted Crystallization Processed Methylammonium Bismuth Iodide Cuboids towards Highly Stable Lead-Free Perovskite Solar Cells. *Energy Environ. Sci.* 2017, 2, 1578–1585.
87. Liu, Z.; Chen, M.; Wan, L.; Liu, Y.; Wang, Y.; Gan, Y.; Guo, Z.; Eder, D.; Wang, S. Anti-solvent spin-coating for improving morphology of lead-free (CH₃NH₃)₃Bi₂I₉ perovskite films. *SN Appl. Sci.* 2019, 1, 706.

88. Konstantakou, M.; Perganti, D.; Falaras, P.; Stergiopoulos, T. Anti-Solvent Crystallization Strategies for Highly Efficient Perovskite Solar Cells. *Crystals* 2017, 7, 291.
89. Corsini, F.; Griffini, G. Recent progress in encapsulation strategies to enhance the stability of organometal halide perovskite solar cells. *JPhys Energy* 2020, 2, 031002.
90. Li, Q.; Song, T.; Zhang, Y.; Wang, Q.; Yang, Y. Boosting Photocatalytic Activity and Stability of Lead-Free Cs₃Bi₂Br₉ Perovskite Nanocrystals via In Situ Growth on Monolayer 2D Ti₃C₂T_x MXene for C–H Bond Oxidation. *ACS Appl. Mater. Interfaces* 2021, 13, 27323–27333.
91. Sun, Q.; Ye, W.; Wei, J.; Li, L.; Wang, J.; He, J.-H.; Lu, J.-M. Lead-free perovskite Cs₃Bi₂Br₉ heterojunctions for highly efficient and selective photocatalysis under mild conditions. *J. Alloys Compd.* 2022, 893, 162326.
92. Bresolin, B.-M.; Sgarbossa, P.; Bahnemann, D.W.; Sillanpää, M. Cs₃Bi₂I₉/g-C₃N₄ as a new binary photocatalyst for efficient visible-light photocatalytic processes. *Sep. Purif. Technol.* 2020, 251, 117320.
93. Guo, Y.; Liu, G.; Li, Z.; Lou, Y.; Chen, J.; Zhao, Y. Stable Lead-Free (CH₃NH₃)₃Bi₂I₉ Perovskite for Photocatalytic Hydrogen Generation. *ACS Sustain. Chem. Eng.* 2019, 7, 15080–15085.
94. Wu, D.; Zhao, X.; Huang, Y.; Lai, J.; Yang, J.; Tian, C.; Hea, P.; Huang, Q.; Tang, X. Synthesis and CO₂ Photoreduction of Lead-Free Cesium Bismuth Halide Perovskite Nanocrystals. *J. Phys. Chem. C* 2021, 25, 18328–18333.
95. Zhou, L.; Xu, Y.-F.; Chen, B.-X.; Kuang, D.-B.; Su, C.-Y. Synthesis and Photocatalytic Application of Stable Lead-Free Cs₂AgBiBr₆ Perovskite Nanocrystals. *Small* 2018, 14, 1703762.
96. Liu, Z.-L.; Liu, R.-R.; Mu, Y.-F.; Feng, Y.-X.; Dong, G.-X.; Zhang, M.; Lu, T.-B. In Situ Construction of Lead-Free Perovskite Direct Z-Scheme Heterojunction Cs₃Bi₂I₉/Bi₂WO₆ for Efficient Photocatalysis of CO₂ Reduction. *Sol. RRL* 2021, 5, 2000691.
97. Otero-Martínez, C.; Fiuza-Maneiro, N.; Polavarapu, L. Enhancing the Intrinsic and Extrinsic Stability of Halide Perovskite Nanocrystals for Efficient and Durable Optoelectronics. *ACS Appl. Mater. Interfaces* 2022, 14, 34291–34302.

Retrieved from <https://encyclopedia.pub/entry/history/show/86386>